Supporting Information

Watschinger et al. 10.1073/pnas.1414887112

SI Materials and Methods

Preparation and Culture Conditions of Bone Marrow-Derived Macrophages. All animal studies were conducted with ethical approval from the Local Ethical Review Committee and in accordance with UK Home Office regulations [Guidance on the Operation of the Animals (Scientific Procedures) Act, 1986]. Bone marrow was obtained from femur and tibia of C57bl/6J mice. Single cells were prepared by passing the suspension through a 70-μm cell strainer. Cells were then cultured in 10-cm dishes for 7 d in 10 mL DMEM:F12 (Invitrogen) supplemented with 100 U/mL penicillin and 100 ng/mL streptomycin (Sigma), 10% (vol/vol) FBS (PAA Laboratories), 5 mM L-glutamine (Sigma), and 10–15% (vol/vol) L929 conditioned medium at 37 °C and 5% CO_2. On day 5, another 5 mL complete culture medium was added.

Differentiation of Bone Marrow-Derived Macrophages. After 7 d in culture, macrophages were plated in six-well plates at a concentration of 2×10^6 cells in 1 mL Opti-MEM (Invitrogen) supplemented with 100 U/mL penicillin, 100 ng/mL streptomycin, and 0.2% (wt/vol) low-endotoxin BSA (Sigma). Two hours after plating, macrophages were stimulated with 10 ng/mL IFN-γ (PeproTech) + 100 ng/mL LPS (Sigma) (for M1) and with 20 ng/mL IL-4 (PeproTech) (for M2). Parallel wells were left unstimulated (M0). After 24 h, cytokines were added fresh. After 48 h of cytokine incubation, cells were collected for (*i*) activity assays by applying two washes with ice-cold PBS before harvesting them using a cell scraper, snap-freezing as a dry-pellet, and storing at −80 °C and (*ii*) gene expression studies by washing them once with ice-cold PBS, harvesting them into 350 μL buffer RLT (RNeasy Kit; Qiagen) containing 10 μL/mL β-mercaptoethanol, and subsequently storing them at −80 °C for further analysis.

AGMO Activity Assay. Enzymatic activity was measured as described (1) with the following modifications: Fatty aldehyde dehydrogenase needed for full conversion of the aldehyde to the acid was provided in its recombinant form exclusively in the assay mixture. Murine bone marrow-derived macrophages were not centrifuged after harvest but the assay was performed in whole-cell homogenates instead.

Gene Expression Analysis by Quantitative PCR. Total RNA from RAW264.7 and bone marrow-derived macrophages was prepared using the RNeasy Kit according to the manufacturer's protocol (Qiagen) and transcribed into cDNA using either M-MLV reverse transcriptase (RNase H Minus, Point Mutant; Promega) or SuperScript II reverse transcriptase (Invitrogen) and random hexamer primers. qPCR analysis was performed by TaqMan assay technology using Brilliant III Ultra-Fast QPCR Master Mix (Agilent Technologies) and the Mx3005P qPCR system (Agilent), or Universal Master Mix (Applied Biosystems) and an iCycler iQ (Bio-Rad). Primer sequences were as follows (all purchased from Microsynth): murine AGMO: 5′-CTTTCTTAGGAGTTGACTTTGGCTACT-3′ (sense), 5′-TGTGCTGCCCAGAAAATATTAATC-3′ (antisense), 5′-CTGGTTCCACCGCATGGCTCATG-3′ (probe); human AGMO: 5′-CTGACCTTGACTTCCATTGGATT-3′ (sense), 5′-CAAGCAACGGAGAGTTTCCATA-3′ (antisense), 5′-CTTCTGGATCAAAGACCCAAGGCAGCT-3′ (probe); murine GCH1: 5′-CGAGGAGGAAAACCAGGTGA-3′ (sense), 5′-GCGAGAGCAGAATGGACGA-3′ (antisense), 5′-CTCCCCAAACTGGCGGCTGCTTA-3′ (probe); murine NOS2: 5′-TCCCTCCTGATCTTGTGTTGG-3′ (sense), 5′-CAACCCGAGCTCCTGGAAC-3′ (antisense), 5′-TGACCATGGAGCATCCCAAGTACGAGT-3′ (probe); murine Fizz1: 5′-GTCCTGGAACCTTTC CTGAGATT-3′ (sense), 5′-AGGGAACAAGTTGTAGTCTTCATCCT-3′ (antisense), 5′-TGCCCCAGGATGCCAACTTTGAA-3′ (probe); murine IL-1β: 5′-ACCTGTCCTGTGTAATGAAAGACG-3′ (sense), 5′-TGGGTATTGCTTGGGATCCA-3′ (antisense), 5′-CACACCCACCCTGCAGCTGGAGA-3′ (probe); murine IL-1RA: 5′-CCTTCTGTTTCATTCAGAGGCA-3′ (sense), 5′-GGCTTGCATCTTGCAGGGT-3′ (antisense), 5′-CCTGCCGCCCTTCTGGGAAAA-3′ (probe); murine TGF-β1: 5′-GCTCTTGTGACAGCAAAGATAACAA-3′ (sense), 5′-GGTCGCCCCGACGTTT-3′ (antisense), 5′-CACGTGGAAATCAACGGGATCAGCC-3′ (probe). All expression data were related to either 18S [5′-CCATTCGAACGTCTGCCCTAT-3′ (sense), 5′-TCACCCGTGGTCACCATG-3′ (antisense), 5′-ACTTTCGATGGTAGTCGCCGTGCCT-3′ (probe)] or murine β-actin [5′-CGTGAAAAGATGACCCAGATCA-3′ (sense), 5′-CACAGCCTGGATGGCTACGT-3′ (antisense), 5′-TGAGACCTTCAACACCCCAGCCATG-3′ (probe)]. Additionally, expression of β-actin was quantified using Mouse ACTB Endogenous Control (VIC/MGB Probe, Primer Limited, 4352341E; Applied Biosystems).

Western Blotting. iNOS, arginase-1, and β-tubulin protein expression shown in Fig. 1*F* was analyzed in bone marrow-derived macrophages (5 μg, determined by BCA protein assay; Thermo Scientific) loaded onto a NuPage 4–12% Bis-Tris gel and transferred to PVDF membrane, and the membranes were blocked using 5% (wt/vol) nonfat skim milk powder (Marvel) in PBS. The blocked membranes were incubated with a mouse anti-iNOS antibody (1:10,000 dilution; BD Biosciences), rabbit anti–arginase-1 (1:20,000 dilution; Abcam), or rabbit anti–β-tubulin antibody (1:20,000 dilution; Abcam) followed by an appropriate HRP-conjugated secondary antibody (Promega). Protein bands were visualized by enhanced chemiluminescence (SuperSignal West Pico Chemiluminescent Substrate; Thermo Scientific).

iNOS expression shown in Fig. S1*B* was analyzed in the six RAW264.7 lines (40 μg, determined by Bradford assay). Proteins were separated on 7.5% or 10% SDS/PAGE, blotted onto PVDF membranes, blocked with 5% BSA, and stained with mouse anti-mouse iNOS antibody (1:5,000 dilution; BD Transduction Laboratories) and ECL Plex goat anti-mouse IgG Cy3 (1:1,250 dilution; GE Healthcare). Blots were scanned using a Typhoon 9410 scanner (532 nm excitation, 580 nm emission, BP 30, 270 V photomultiplier voltage; GE Healthcare). Western blot band pixel count was quantified with ImageQuant TL software (GE Healthcare), and iNOS signals were normalized on β-actin signals (mouse anti-actin antibody, clone C4, 1:1,000 dilution; Millipore).

Modulation of AGMO and GCH1 Activity in RAW264.7 Macrophages by Lentiviral Constructs. Short hairpin RNA (shRNA)-encoding oligonucleotides [5′-GAGGTGCCTGATTACGTAA-3′ targeting murine AGMO 506–524 (GenBank accession no. NM_178767.5) for shAGMO506; 5′-CCACAGTTCTGAAGACTAT-3′ targeting murine AGMO 847–865 (GenBank accession no. NM_178767.5) for shAGMO847; 5′-CGTAAGAAGCATAACACAA-3′ targeting murine AGMO 1699–1717 (GenBank accession no. NM_178767.5) for shAGMO1699; and 5′-CCATGCAGTACTTCACCAA-3′ targeting murine GCH1 410–428 (GenBank accession no. NM_008102.3) for shGCH1] were cloned into BglII-HindIII–digested pENTR-THT-III downstream of a modified H1 RNA gene promoter and verified by DNA sequencing. For stable integration of the shRNA, the expression cassette was shuttled

into the lentiviral vector pHR-DEST-Puro as well as pGLTR-DEST-GFP-TetR using a GATEWAY LR clonase-mediated reaction (Invitrogen). The control line shLUC expressing shRNA against luciferase (155–173 from pGL3 Luciferase; Promega) was generated similarly. Infectious lentiviral particles were generated by cotransfection of the lentiviral vectors with the packaging plasmid (pSPAX2) and the pseudotyping vector pVSV-G into HEK293T cells as described previously (2). Twenty-four hours after transfection, media were exchanged for target cell-growth media. Supernatant was harvested at 48 and 72 h after transfection, 0.45 μm-filtered, and added to target cells for 24 h. Infected cells were identified by GFP fluorescence or selected for puromycin resistance (2.5 μg/mL).

For the AGMO-overexpressing line +huAGMO, the ORF of human AGMO together with a 3×FLAG tag was amplified from a plasmid containing the human AGMO reading frame (GenBank accession no. NM_001004320) with a C-terminal 3×FLAG tag using the primers 5′-CAAAAAAGCAGGCTCC-GCCACCATGGGAGACCGCGG-3′ and 5′-CAAGAAAGCTGG-GTCTTAAACCCGGGATCCTCTAG-3′. The purified PCR product was reamplified using the primers 5′-GGGGACAA-GTTTGTACAAAAAAGCAGGCTCC-3′ and 5′-GGGGACC-ACTTTGTACAAGAAAGC TGGGTC-3′ to flank the ORF with attB1 and attB2 sites, respectively. The PCR product was again gel-purified and recombined into pDONR207 (Invitrogen) using a BP clonase reaction to generate an ENTR vector, which was verified by DNA sequencing. The AGMO gene was then transferred from the ENTR vector into pHR-SFFV-DEST-ires Puro to generate a lentiviral expression vector.

RAW264.7 Cell Culture. All RAW264.7 lines were cultured at 37 °C under 5% CO_2 in VLE-Dulbecco's MEM nutrient medium (Biochrom) supplemented with 10% (vol/vol) heat-inactivated FBS (Sigma). Cells were harvested for activity assays and gene expression studies in analogy to the bone marrow-derived macrophages.

Live-Cell Assay for Quantification of Pyrenedecanoic Acid Formation. RAW264.7 cells were cultivated in 1 μg/mL doxycycline ± 1 μM sepiapterin (SP) for 3 d and plated in six-well plates at a density of 2×10^6 per well in 2 mL medium (+doxycycline ± SP). After 48 h, cells were scraped off, resuspended in 250 μL culture medium containing 5 μM 1-*O*-pyrenedecyl-*sn*-glycerol (synthesized according to ref. 3) or 5 μM pyrenedecanoic acid (Sigma), and transferred to a 96-well plate by maintaining the same cell number per well area. The tetrahydrobiopterin precursor SP (Schircks Laboratories) was added in a concentration range up to 5 μM from a 100-μM stock solution in PBS where indicated.

After selected time points, 10 or 20 μL supernatant of each well was taken and mixed with three volumes of methanol to stop the reaction. The mixture was centrifuged for 10 min at 4 °C and 13,000 × *g*, and 10 μL was then injected onto an Agilent 1200 Series HPLC system [column: Zorbax XDB-C8, 4.6 × 50 mm, 3.5 μm particle size; Agilent Technologies; elution: 21% (vol/vol) 10 mM potassium phosphate buffer (pH 6.0) and 79% (vol/vol) methanol for 4.5 min, followed by a gradient to 100% methanol at 5.0 min; at 8.0 min the initial buffer/methanol mix was reestablished and the column was equilibrated until 8.5 min; flow rate: 1 mL/min; detection by fluorescence (excitation 340 nm, emission 400 nm)]. Quantification of pyrenedecanoic acid was achieved by integration of the area below the curve and relating it to a pyrenedecanoic acid standard. The decrease in medium volume by multiple removals of samples was taken into account. Cell viability was tested using a 3-(4,5-dimethylthiazol-2-yl)-2,5-diphenyltetrazolium bromide test (Promega) according to the manufacturer's recommendations.

GCH1 Activity Assay. Low-molecular mass compounds were removed by Sephadex G-25 chromatography (NAP-5 columns; GE Healthcare), and cellular protein was eluted from the column in 0.1 M Tris·HCl buffer (pH 7.8) containing 0.3 M KCl, 10% (vol/vol) glycerol, and 2.5 mM EDTA. Eluted protein was then incubated with 2 mM GTP (Sigma) at 37 °C for 90 min to generate 7,8-dihydroneopterin triphosphate, which was subsequently oxidized by acidic iodine and cleaved by alkaline phosphatase (Sigma). Resulting neopterin was then quantified by HPLC as described (4). Protein amount was measured by Bradford assay (5) (Bio-Rad) and GCH1 activity was normalized to it.

Tetrahydrobiopterin Concentration. Cellular tetrahydrobiopterin was quantified using iodine oxidation of supernatants in acid and base by a method modified from Fukushima and Nixon (6). Twenty microliters of ascorbate-treated mixture was injected onto a Nucleosil 10 SA column (4 × 250 mm long; Macherey-Nagel) and eluted with 50 mM potassium phosphate buffer (pH 3.0) at a flow rate of 1.5 mL/min, and biopterin was detected by fluorescence (excitation 350 nm, emission 440 nm). Tetrahydrobiopterin concentrations were calculated as the difference of quantified biopterin species in acidic and basic oxidation conditions. Protein amount was quantified by Bradford assay and tetrahydrobiopterin levels were normalized to it.

Nitrite in RAW264.7 Supernatants. To quantify nitrite levels in the supernatants, 50 μL freshly taken supernatant was mixed with 75 μL distilled water and 125 μL Griess-Ilosvay reagent (Merck) and incubated for 10 min, and the pink color was quantified by photometric readings at 562 nm. $NaNO_2$ was used as standard (2.5–100 μM).

Lipid Extraction from Cells. For intracellular lipid analysis, we used five cell lines in pentaplicates: shLUC, shAGMO506 (=shAGMO), +huAGMO, shGCH1, and shGCH1 +SP. Low-binding Eppendorf tubes were used for the extraction/centrifugation steps and glassware was used for storage. Pellets from ~7×10^6 RAW264.7 cells (corresponding to ~450 μg of cellular protein) were mixed with 100 mg glass beads (425–600 μm in diameter; Sigma) and 10 μL internal standard (PAF-d_4 or lyso-PAF-d_4; Cayman; stock concentration 2 μM in methanol) was added. After addition of 500 μL chloroform/methanol 2:1 (vol/vol) and shaking at 4 °C in a Mixer Mill MM 400 (Retsch) using four cycles of 30 s at 20 Hz, 100 μL distilled water was added, mixed on a vortex for 30 s, and centrifuged for 10 min at 26,900 × *g* and 4 °C. The organic (bottom) phase was transferred to a brown glass vial and the remaining water phase was extracted again by adding 500 μL chloroform/methanol 2:1 (vol/vol). The organic phases were combined and dried in a fume hood overnight, and lipids were taken up in 100 μL isopropanol/acetonitrile/water 2:1:1 (vol/vol/vol), transferred to glass autosampler vials with glass inlets, and stored at −80 °C until analysis. Samples included five parallels each for shLUC, shAGMO506, +huAGMO, shGCH1, and shGCH1 +SP. Cell counts and protein amounts were quantified from parallel culture wells to check for potential differences in the amount of cells collected after the cultivation period, such as due to different growth rates. Cell counts and protein amounts were highly comparable among the five groups, and measurement of alkylglycerol monooxygenase activity and tetrahydrobiopterin content confirmed the expected behavior of the different treatment regimens in the cells collected for lipidomic analysis (Table S1).

Targeted LC-MS/MS Analysis. Extracted lipid samples were separated on an LC system (Agilent 1290) using a Zorbax Eclipse Plus C18, Rapid Resolution HD (2.1 × 100 mm, 1.8 μm particle size; Agilent; column temperature: 20 °C; injection volume: 1 μL with flush port needle wash). The column was equilibrated with 25% buffer A [acetonitrile/water (1:1), 10 mM ammonium acetate] and buffer B (100% acetonitrile). Compounds were eluted in a gradient to 100% B within 7 min. After a washing step at 100% B for 1 min, the initial mobile-phase composition was reestablished

within 1 min and the column was equilibrated for 2 min for the following injection. This resulted in a total cycle time of 11 min.

Identification and quantification of the lipid metabolites were accomplished with an online-coupled triple-quadrupole mass spectrometer (Agilent 6460) working in multiple reaction monitoring (MRM) mode (dwell time: 25 ms) by matching fragmentation pattern and retention time with commercially available pure standards. Transitions as well as ionization and fragmentation energies were, when possible, optimized for each metabolite individually using pure standards or estimated from their chemically nearest neighbor (as indicated in Table S4*A*). MRM transitions and fragmentation settings are given in Table S4*A*. Ion-source settings can be found in Table S4*B*.

Raw data were analyzed with a MassHunter Workstation (Agilent). The automated peak integration was verified manually, and peaks with an unfavorable signal-to-noise ratio were rejected. Isotope-labeled internal standards (PAF-d_4 and lyso-PAF-d_4; Cayman) as well as spiking experiments with unlabeled standards were used for peak identification. Absolute lipid concentrations were calculated with the help of external calibration curves. A possible instrumental drift could be excluded with repeatedly measured quality controls. Concentration data were exported from the MassHunter software and analyzed with R (www.R-project.org).

Untargeted LC-MS Lipidomics. Total lipid analysis was performed with an ionKey/MS system composed of an ACQUITY UPLC M-Class, the ionKey source, and an iKey CSH C18 130 Å, 1.7 μm particle size, 150 μm × 100 mm column (Waters) coupled to a SYNAPT G2-Si (Waters). The capillary voltage was 2.8 kV and the source temperature was 110 °C. Injections were 0.5 μL using partial-loop mode with a column temperature of 55 °C and a flow rate of 3 μL/min. Mobile phase A consisted of acetonitrile/water (60:40) with 10 mM ammonium formate + 0.1% formic acid. Mobile phase B consisted of isopropanol/acetonitrile (90:10) with 10 mM ammonium formate + 0.1% formic acid. The gradient was programmed as follows: 0.0–2.0 min from 40% B to 43% B, 2.0–2.1 min to 50% B, 2.1–12.0 min to 99% B, 12.0–12.1 min to 40% B, and 12.1–14.0 min at 40% B. For the untargeted analysis, a mass range of 50–1,500 *m/z* was selected in both positive and negative electrospray ionization modes.

Data Processing and Analysis. For the untargeted lipidomic approach, a combination of analysis of the variance (ANOVA) and multivariate statistics, including principal-component analysis (PCA) and partial, least-squares discriminant analysis, identified lipids most responsible for differences between our sample groups. Compounds were identified by database searches as performed by Human Metabolome Database version 3.5 (HMDB; www.hmdb.ca) (7) and LIPID MAPS (www.lipidmaps.org) as well as by fragmentation patterns, retention times, and ion mobility-derived collision cross-sections versus commercially available reference standards, when available. Five hundred and eighty-one unique masses (retention time and *m/z*) from positive ESI mode could be mapped to 12,026 possible compound IDs, and 448 unique masses from negative ESI mode were mapped to 5,443 possible IDs (17,469 possible IDs in total). We removed the redundant information from the HMDB for compounds that had possible identification from the LIPID MAPS database. A large number of IDs were also redundant in both, individual ESI mode as well as in a combination of both. Unique compound IDs from positive ESI mode were 6,168, whereas unique compound IDs from negative ESI mode were 3,498, and by combining together we obtained 8,164 unique IDs from both positive and negative ESI mode belonging to 1,029 lipid compounds in total.

Univariate analyses (Student's *t* tests) were conducted to assess for significance (*P* value). Data processing and analysis were conducted using Progenesis QI (Nonlinear Dynamics). Data quantification was performed using TargetLynx software (Waters).

PCA and Cluster Analysis of AGMO Knockdown and Overexpression. Significantly altered lipid profiles measured in positive and negative ESI mode were combined. All conditions were measured in biological pentaplicates ($n = 5$), except for one replicate in negative ionization mode in the shAGMO506 condition ($n = 4$). PCA (Fig. S4) was performed to evaluate variance and structure. Z scores of the averaged lipid profiles were calculated and used to determine the Euclidean distances between these profiles by hierarchical clustering. The resultant distance matrix was used to divide the lipids into eight groups according to similarities in their concentration profiles. Each group was then subjected to lipid category, class, and subclass enrichment analysis separately as described below.

Lipid Enrichment Analysis in RAW264.7 with AGMO and GCH1 Modulation. In total, 1,029 lipid compounds from both positive and negative ESI mode were identified from HMDB version 3.5 and LIPID MAPS, out of which 378 and 176 compounds had significantly altered lipid profiles compared with control from both AGMO and GCH1 manipulation experiments, respectively. Some compounds were mapped to more than one ID belonging to multiple categories/classes/subclasses. In cases of incompatibility between the annotation in the HMDB and LIPID MAPS, redundant information from HMDB annotation was removed for compounds that had possible identification from the LIPID MAPS database. When possible, identified HMDB annotations were curated to match with the respective categories, classes, and subclasses of the LIPID MAPS database, or were assigned to a separate "unclear" category/class/subclass. For every category/class/subclass, the number of significantly altered compounds was counted from the list of all possible identifications, and enrichment analysis was performed to examine for significantly altered category/class/subclass by using a hypergeometric test. For significance criteria, a *P* value cutoff of 0.01 and a number of compounds for every category/class/subclass more than two were used. Category/class/subclass enrichment analysis was performed separately for manipulation of AGMO and GCH1 activities and for all eight clusters identified based on similar profiles in the AGMO dataset (as described above).

Statistical Analysis. Unless indicated otherwise, data are presented as means ± SEM. Data were compared by Student's *t* test and one-way ANOVA with Bonferroni's multiple comparison, as mentioned in the figure legends, using GraphPad Prism 5.01. *P* values <0.05 were considered statistically significant.

1. Watschinger K, et al. (2012) Catalytic residues and a predicted structure of tetrahydrobiopterin-dependent alkylglycerol mono-oxygenase. *Biochem J* 443(1):279–286.
2. Sigl R, Ploner C, Shivalingaiah G, Kofler R, Geley S (2014) Development of a multipurpose GATEWAY-based lentiviral tetracycline-regulated conditional RNAi system (GLTR). *PLoS ONE* 9(5):e97764.
3. Werner ER, Hermetter A, Prast H, Golderer G, Werner-Felmayer G (2007) Widespread occurrence of glyceryl ether monooxygenase activity in rat tissues detected by a novel assay. *J Lipid Res* 48(6):1422–1427.
4. Werner ER, Wachter H, Werner-Felmayer G (1997) Determination of tetrahydrobiopterin biosynthetic activities by high-performance liquid chromatography with fluorescence detection. *Methods Enzymol* 281:53–61.
5. Bradford MM (1976) A rapid and sensitive method for the quantitation of microgram quantities of protein utilizing the principle of protein-dye binding. *Anal Biochem* 72: 248–254.
6. Fukushima T, Nixon JC (1980) Chromatographic analysis of pteridines. *Methods Enzymol* 66:429–436.
7. Wishart DS, et al. (2013) HMDB 3.0—The Human Metabolome Database in 2013. *Nucleic Acids Res* 41(Database issue):D801–D807.

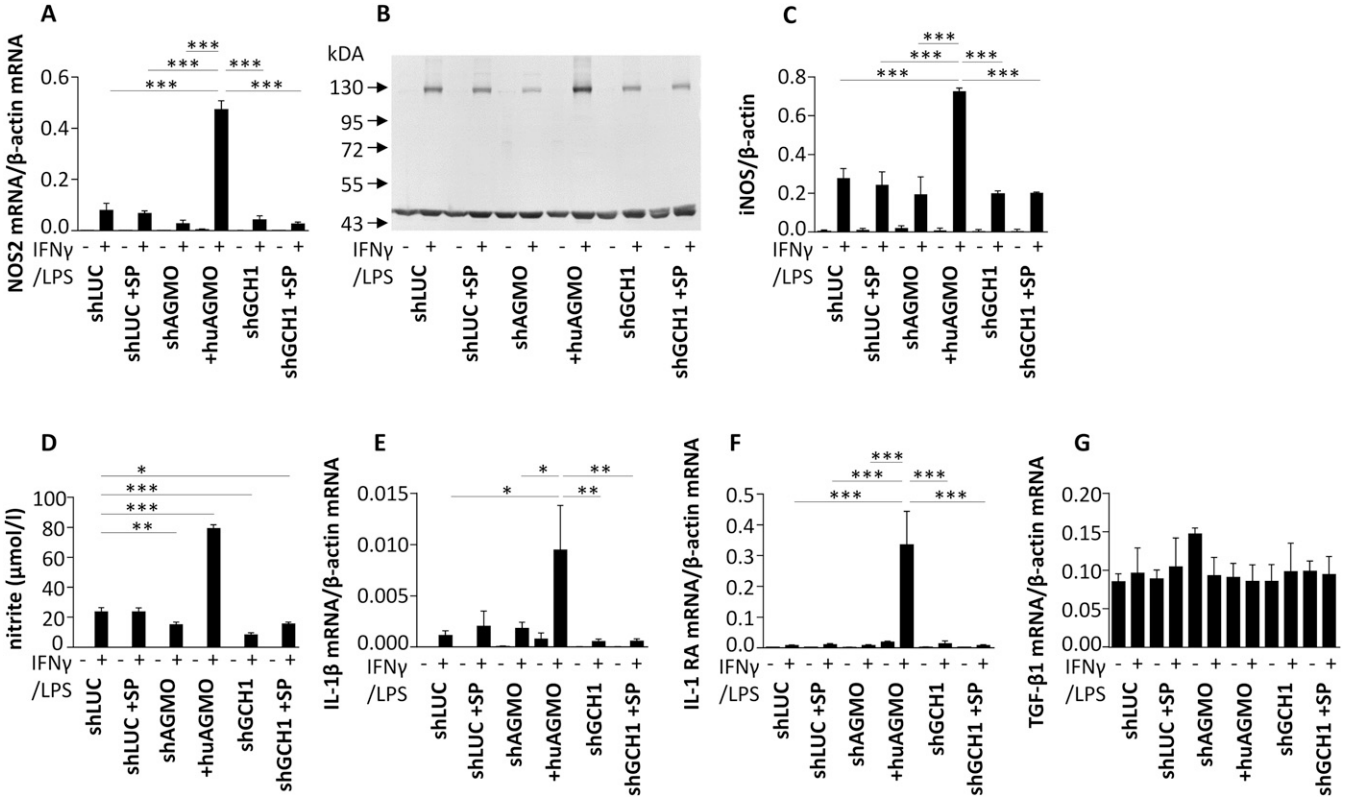

Fig. S1. Analysis of the impact of IFN-γ/LPS stimulation and AGMO and GCH1 modulation in RAW264.7 cells on nitric oxide synthase and selected cytokines. (*A*) Analysis of NOS2 gene expression using qPCR and TaqMan technology. Data were normalized to β-actin. (*B*) Representative Western blot of iNOS protein expression (130.6 kDa). Protein marker bands are indicated by arrows, and the respective size is given in kDa. β-Actin was used as loading control. (*C*) Bar graph showing iNOS expression obtained by Western blots normalized to β-actin expression. (*D*) Nitrite was quantified in supernatants using Griess-Ilosvay reagent. (*E*) Analysis of IL-1β gene expression using qPCR and TaqMan technology. Expression data were normalized to β-actin. (*F*) Analysis of IL-1RA gene expression using qPCR and TaqMan technology. Expression data were normalized to β-actin. (*G*) Analysis of TGF-β1 gene expression using qPCR and TaqMan technology. Expression data were normalized to β-actin. Data are presented as means ± SEM. Statistical analysis was performed using one-way ANOVA and Bonferroni's multiple comparisons. $*P < 0.05$, $**P < 0.01$, $***P < 0.001$. Data were obtained in at least three independent experiments.

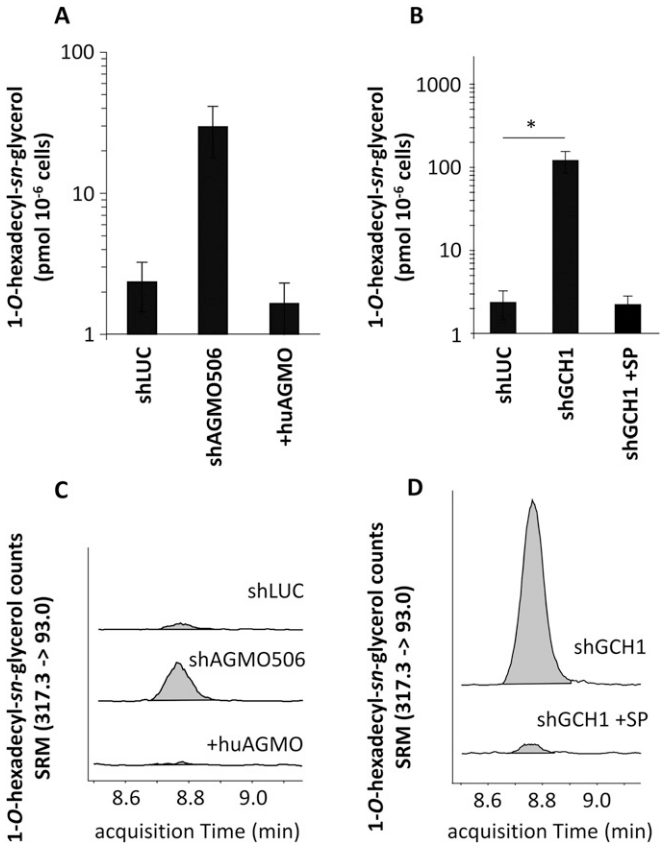

Fig. S2. Targeted analysis of the direct AGMO substrate 1-*O*-hexadecyl-*sn*-glycerol in RAW264.7 with modulated AGMO and GCH1 activity. (*A*) AGMO activity was modulated in RAW264.7 cells using lentiviral shRNA constructs. An LC-MS/MS (MRM; three specific transitions) method was used to determine intracellular concentrations of 1-*O*-hexadecyl-*sn*-glycerol, a known substrate of AGMO. AGMO knockdown (shAGMO506) resulted in accumulation of this ether lipid when compared with control cells (shLUC), whereas respective levels were near the limit of detection upon AGMO overexpression (+huAGMO). (*B*) Knockdown of the biosynthesis of the AGMO cofactor tetrahydrobiopterin led to a comparable accumulation of 1-*O*-hexadecyl-*sn*-glycerol in shGCH1. This effect could be reversed by supplementation with sepiapterin (shGCH1 +SP), which can restore tetrahydrobiopterin levels in a GCH1-independent manner. Data are presented as means ± SEM. $*P < 0.05$. (*C* and *D*) Raw chromatograms of one 1-*O*-hexadecyl-*sn*-glycerol transition (317.3→93.0) for AGMO and GCH1 manipulations are shown in *C* and *D*, respectively.

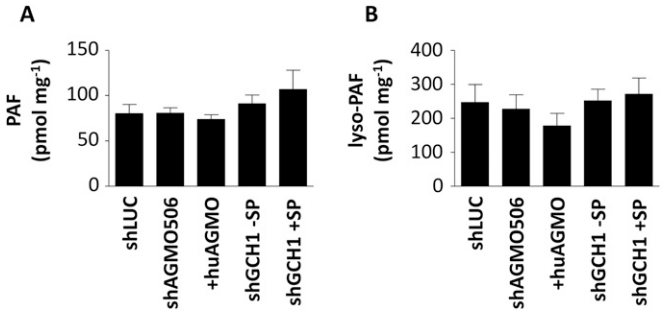

Fig. S3. Targeted analysis of PAF and lyso-PAF in RAW264.7 with modulated AGMO and GCH1 activity. PAF (*A*) and lyso-PAF (*B*) were quantified with the use of deuterated standards in lipid extracts of RAW264.7 cells manipulated by knockdown and overexpression of AGMO, as well as knockdown of GCH1 with and without addition of sepiapterin, and related to protein levels of cells grown in parallel wells on the same plate. When calculated based on cell counts (Table S1) as in ref. 1 and compared with the values shown in this reference for untreated RAW264.7 cells, exactly similar concentrations were found for lyso-PAF (3.27 ± 0.23 ng per 4×10^5 cells, $n = 25$) and slightly higher levels for PAF (1.34 ± 0.13 ng per 4×10^5 cells, $n = 25$). Data are presented as means ± SEM. Data were obtained in five independent experiments.

1. Tokuoka SM, Kita Y, Shindou H, Shimizu T (2013) Alkylglycerol monooxygenase as a potential modulator for PAF synthesis in macrophages. *Biochem Biophys Res Commun* 436(2):306–312.

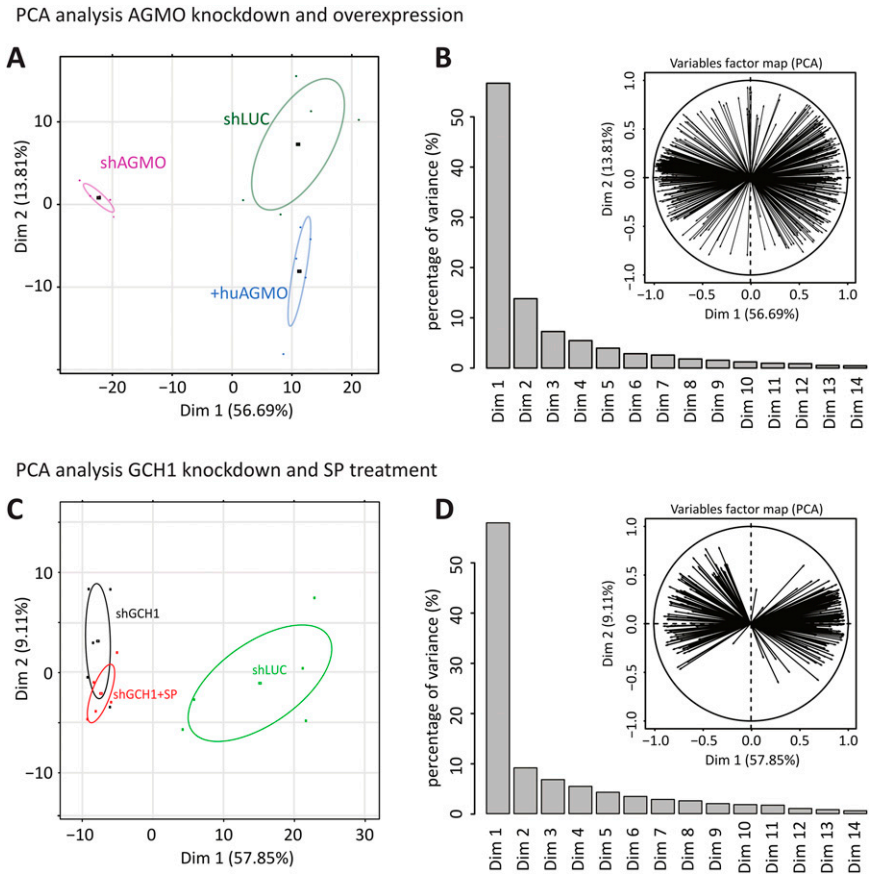

Fig. S4. Principal-component analysis (PCA) of lipidomic data. (*A*) Each dot represents one of the five replicate samples in a multidimensional lipid metabolite peak area space projected on the principal plane formed by the first two principal axes (Dim 1 and Dim 2), covering 56.69% and 13.81% of the variance, respectively. The dots are colored according to their sample group (shAGMO, shLUC, and +huAGMO). Separation of AGMO knockdown is mainly described by Dim 1, whereas Dim 2 separates the AGMO overexpression condition (+huAGMO). (*B*) Percentage of variance explained by the individual principal components. (*Inset*) Subplot depicts the variables vector map for the contributions of the individual lipid species to the principal components Dim 1 and Dim 2. (*C*) As described in *A*, with the difference that sample groups for GCH1 manipulation were used (shGCH1, shLUC. and shGCH1 +SP). (*D*) As in *B*, with the difference that sample groups for GCH1 manipulation were used.

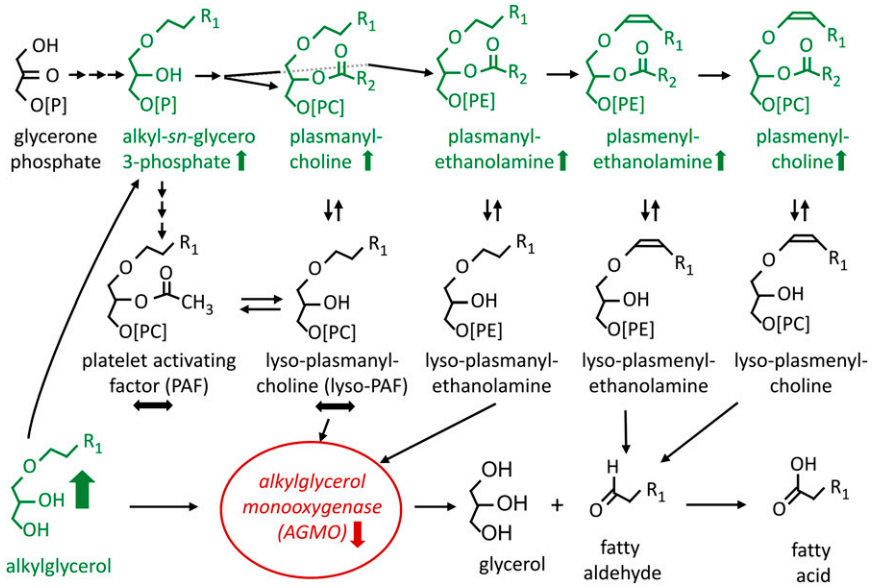

Fig. S5. Metabolic scheme of the impact of AGMO knockdown on ether lipid metabolism. Ether lipids are synthesized in the body from glycerone phosphate. Knockdown of AGMO (red arrow) leads to an accumulation of free alkylglycerols, the direct substrates of AGMO. The accumulation of ether lipids (green arrows) upon AGMO knockdown can be explained by known anabolic pathways of the accumulating free alkylglycerol. PAF and lyso-PAF, however, are not influenced by modulation of AGMO in our experiments (black arrows). Note that the altered species represent only a part of the observed changes.

Table S1. Protein amount and cell count of the five RAW264.7 cell lines analyzed in lipidomics

Table S1

The five cell lines shLUC, shAGMO, +huAGMO, shGCH1, and shGCH1 +SP were harvested and wells grown in parallel to the ones used for lipid extraction and lipidomics analysis were used to analyze protein content, cell count, AGMO activity, and tetrahydrobiopterin content. Values show mean ± SD of five determinations.

Table S2. Lipid enrichment analysis for AGMO and GCH1 manipulation in RAW264.7 cells

Table S2

Enrichment analysis of categories, classes, and subclasses was performed for AGMO and GCH1 datasets by applying a hypergeometric test. "p-value" indicates how significantly a category, class, or subclass is enriched, and "# sign." is the number of lipid species with significantly altered profile, out of the total number of lipid species in a particular category, class, or subclass ("# total").

Table S3. Cluster-specific lipid category, class, and subclass enrichment for AGMO and GCH1 manipulation in RAW264.7 cells

Table S3

(*A*) Cluster-specific lipid category enrichment. The lipid profile of the AGMO dataset was clustered among eight clusters, and enrichment analysis of categories was performed by hypergeometric test for every cluster. "p-value" indicates how significantly a category is enriched in a cluster. "# of IDs" represents the total number of lipid species with significantly altered profile belonging to a category, and the last column "ratio: sign/total IDs" is the ratio of the significantly altered profile with respect to the total number of observed lipid species (both significantly and nonsignificantly) for the category. (*B*) Cluster-specific lipid class enrichment. The lipid profile of the AGMO dataset was clustered among eight clusters, and enrichment analysis of classes was performed by hypergeometric test for every cluster. p-value indicates how significantly a class is enriched in a cluster. # of IDs represents the total number of lipid species with significantly altered profile belonging to a class, and the last column ratio: sign/total IDs is the ratio of the significantly altered profile with respect to the total number of observed lipid species (both significantly and nonsignificantly) for the class. (*C*) Cluster-specific lipid subclass enrichment. The lipid profile of the AGMO dataset was clustered among eight clusters, and enrichment analysis of subclasses was performed by hypergeometric test for every cluster. p-value indicates how significantly a class is enriched in a cluster. # of IDs represents the total number of lipid species with significantly altered profile belonging to a class, and the last column ratio: sign/total IDs is the ratio of significantly altered profile with respect to the total number of observed lipid species (both significantly and nonsignificantly) for the subclass.

Table S4. SRM transitions and mass-spectrometer parameters

Table S4